Hindawi

Research Article

Finite Element-Based Performance Analysis of Encased Composite Columns under Monotonic Axial Compression Load

Kefiyalew Zerfu [1] **and Regasa Yadeta** [2]

[1]*Department of Civil Engineering, Jimma Institute of Technology, Jimma University, Ethiopia*
[2]*Department of Civil Engineering, College of Engineering and Technology, Mettu University, Ethiopia*

Correspondence should be addressed to Kefiyalew Zerfu; kefiyalewz@gmail.com

This paper presents the results of an investigation into the performance of fully encased composite columns under monotonic axial load using finite element simulation. The damage characteristics and the performance investigation of the specimen were mainly focused on the influence of the compressive strength of concrete and the size of reinforcement. The concrete material was modeled using concrete damage plasticity (CDP), which incorporates the hardening and softening behaviors, and the steel was modeled using metal plasticity. The results obtained from the current study were validated by using previously conducted experimental work and manual calculation based on Eurocode 4. According to the FEA result, damage to the concrete matrix was significantly minimized with the increase in the strength of the concrete. By keeping other parameters constant, an increase in longitudinal reinforcement diameter minimizes the equivalent plastic strain both in structural steel and reinforcement bars. Furthermore, the results showed that the numerical simulation fairly validated the analytical solution.

1. Introduction

Due to its structural performance, especially in high-rise buildings and seismic-prone areas, composite construction is getting attention globally. Better functional and performance requirement of structural system is achieved by the utilization of steel-concrete structure. Due to their superior structural performance compared with conventional reinforced concrete (RC) columns, concrete-encased steel (CES) composite columns are gaining popularity in top-down or basement construction [1–3]. An advantage of composite structure construction is that the structure acquires its strength from the combined resistance of concrete and steel. Steel structures usually have improved ductility, high strength-to-weight, and stiffness-to-weight ratios [4–7]. Proper use of composite construction results in reductions in initial and life-cycle costs [8, 9]. High costs in the construction industry mainly occur due to labor costs and on-site temporary works. In the case of a high-rise building and bridge construction, the construction cost and time of

temporary works significantly affect the effectiveness of conventional reinforced concrete construction. The construction process of reinforced concrete columns passes one of the critical paths. Thus, there is a need to reduce the cost and time of the on-site temporary works in the construction industry during the construction period [10, 11]. Composite construction, such as encased composite columns, is the most widely used type of composite construction. A fully encased composite column (FEC) provides improved strength, stability, stiffness, fireproofing, and corrosion protection [12–15].

Basically, a steel-concrete composite column comprises either a concrete-encased steel section or a concrete-filled tubular steel section. Steel-concrete composites are generally used as load-bearing members in a composite-framed structure. The combined resistance to external loading in a composite column is enhanced by providing supplementary reinforcement. This prevents excessive spalling of the concrete under external load and fire conditions [16, 17]. So far, many studies have been

conducted to study the performance of composite columns under different loading conditions, including combined action [1, 13, 18–24]. In addition, concrete-filled steel tubes under cyclic load were also reported in previous studies [24–26]. Previous studies showed that there are different factors that influence the performance of the composite column. For instance, an increase in the compressive strength of concrete yields an improved capacity for the composite column [4, 27–29]. The provision of confinement has also an effect on the load-carrying capacity, which depends on the steel section shape and the spacing between the transverse reinforcements [1, 30–32]. The effects of cross-section, column height, and confinement were also reported for different eccentricities and structural steel shapes [33–36]. Previous studies conducted on experimental and analytical studies of square composite columns with two interlocking spirals revealed an improved axial compressive capacity and ductility behavior of composite columns. The utilization of a circular and star-shaped spiral enhances the confinement effect for the core concrete [23, 24, 37–39]. According to Jin et al. [40], the constraint effect under concrete is enhanced as the confinement increases and the failure behavior of the column becomes less brittle. The cross-section of steel tubes and the addition of steel fiber also matter for the performance of a composite column. Zhang et al. [41] stated that the utilization of circular steel tubes is recommended over a square steel tube to meet the desired design strength requirement and provide better confinement to core concrete. Furthermore, Zhang et al. [41] quantified that the utilization of steel fibers effectively improved the ductility and reduced the crack width.

Finite element analysis (FEA) is a widely utilized method to study the performance and failure characteristics of engineering structures. This computer-based analysis also helps to study the complex behavior that accounts for the material and geometric nonlinearity of steel-concrete composite columns. Earlier studies showed that FEA can fairly validate the results obtained from experimental tests [42–48]. The study result reported by Shih et al. [23] for a fully encased composite column (FEC) made of high-strength steel and concrete stated that finite element analysis reasonably validated the experimental result. Ellobody and Young [43] and Lai et al. [49] also quantified the nonlinear 3-D finite element model as an important tool to evaluate the performance of composite columns. Finite element analysis is applied to investigate the complex load transfer mechanism in composite structures such as a concrete-encased column [13, 18, 24, 50].

The focus of this study is to investigate the damage and performance characteristics of an encased composite column under monotonic axial load. The strength of the concrete and the size of the reinforcing bars were used as the main parameters in this study. Nonlinear finite element analysis (FEA) was conducted for the damage behavior and load-carrying capacity of the composite column. Analytical design checks were carried out based on the simplified design method of the Eurocode 4 (EC4) plastic design

approach. The FEA and analytical result verifications were conducted by comparing the experimental test reported by Lai et al. [1].

2. Material Data and Test Specimens

2.1. Material Data. The material definition and an appropriate material model is a crucial element in finite element modeling. The material properties for concrete structural steel and reinforcing bars should be defined with appropriate material parameters. During the finite element analysis, the nonlinear material behavior of these materials was included in the numerical simulation. The comprehensive details of material models were described in the following sections.

2.1.1. Concrete Compressive Strength. Four classes of cylindrical compressive strength were utilized in this study, as shown in Table 1. The concrete specimen having a compressive strength of 52.3 MPa was adopted from an experimental test reported by [1]. The encased composite column specimen with this compressive strength was used as a control for the validation study under the current study. However, the remaining concrete compressive strength classes were utilized as additional study parameters for the performance investigation of the encased composite columns. The modulus of elasticity and Poisson's ratio of these specimens were calculated based on Eurocode-2 provisions for the design of concrete structures [51].

2.1.2. Damage Plasticity Modeling. ABAQUS© software offers mainly the following three crack model options to simulate the damage behavior of concrete(1) smeared crack model, (2) brittle crack model, and (3) concrete damaged plasticity model. The concrete damaged plasticity model was utilized in this study, incorporating the inelastic behavior of concrete under tension and compression, which incorporates damage parameters [52]. Thus, in ABAQUS© software, the concrete material is usually simulated under static and dynamic loading conditions using the concrete damaged plasticity model [53]. Tensile cracking and compressive crushing are the two main failure mechanisms considered for the damage plasticity model of concrete. The tensile and compressive behavior of concrete under uniaxial load is described by the damaged plasticity model [54]. During modeling, the degradation of the elastic stiffness in tension and compression is considered for analysis. Furthermore, under cyclic loading, stiffness recovery is accounted for by this model. The response of concrete presented in Figure 1 was utilized in the current study [53].

The tensile and compressive damage parameters, (d_c) and (d_t), are calculated by equations (1) and (2), respectively. The value for the scalar damage variables, d_t and d_c, ranges from 0 (undamaged) to 1 (fully damaged) [55]. The compressive crushing and tensile cracking failure processes are considered in the damage model based on concrete plasticity.

TABLE 1: Mechanical properties of concrete.

Concrete grade	Cylindrical compressive strength (MPa)	Modulus of elasticity (GPa)	Poisson's ratio	Remark
C50	52.3	32.9	0.2	*
C25	25	31	0.2	**
C30	30	33	0.2	**
C35	35	34	0.2	**

*Mechanical properties of concrete from experimental work [1]. **Mechanical properties of concrete based on Eurocode-2 provision [51].
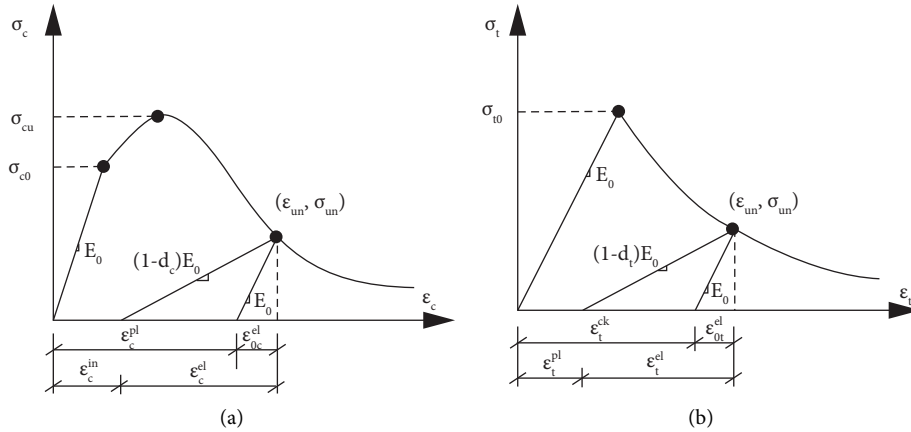

FIGURE 1: Stress-strain behavior [53]: (a) compression and (b) tension.

$$\sigma_t = (1 - d_t)E_O\left(\varepsilon_t - \varepsilon_t^{pl}\right), \tag{1}$$

$$\sigma_c = (1 - d_c)E_O\left(\varepsilon_c - \varepsilon_c^{pl}\right). \tag{2}$$

The strain hardening and softening behavior of the concrete were considered for the reinforced concrete during the analysis. To incorporate the complete tensile behavior of reinforced concrete, the input data for Young's modulus (E_0), stress (σ_t), cracking strain (ε_{tck}), and the damage parameter (d_t) were considered during the simulation. The cracking strain (ε_{tck}) was calculated from the total strain using the following equation:

$$\varepsilon_t^{ck} = \varepsilon_t - \varepsilon_{ot}^{el}, \tag{3}$$

where $\varepsilon_{ot}^{el} = \sigma_t/E_o$ is the elastic strain and ε_t is the total strain.

Again, the plastic strains are determined from the following equations:

$$\varepsilon_t^{pl} = \varepsilon_t^{ck} - \frac{d_t}{(1 - d_t)} * \left(\frac{\sigma_t}{E_o}\right), \tag{4}$$

$$\varepsilon_c^{pl} = \varepsilon_c^{ck} - \frac{d_c}{(1 - d_c)} \frac{\sigma_c}{E_0}, \tag{5}$$

where E_0 is the initial modulus of elasticity.

Parameters describing the state of the material in which the concrete undergoes failure under biaxial compression were also used in this study. The ABAQUS user's manual specifies that the default value for the ratio of the strength in the biaxial state to the strength in the uniaxial state (f_{b0}/f_{c0}) is

equal to 1.16. The dilation angle, which is the angle of inclination of the failure surface towards the hydrostatic axis, measured in the failure plane, was also considered [24, 53]. The dilation angle, ψ, is physically interpreted as a concrete internal friction angle. Under this study, the dilation angles of $\psi = 32°$, $34°$, $36°$, and $\psi = 38°$ were used for the corresponding concrete grades C25, C30, C35, and C50, respectively.

2.1.3. Steel Material Modeling. The steel materials were modeled as an elastoplastic material as given in Eurocode 3, 2005, Abaqus manual, and Eurocode 2, 2005 [51, 53, 56]. Figure 2 shows the true stress and logarithmic strain graph that was utilized for the modeling of steel materials. To define the nonlinear behavior of the structural steel section and the reinforcement, the metal plasticity model was used. There true strain-stress behavior was used for steel material to account for the nonlinear behavior characteristics, which enable it to capture the postbehavior of the material [56]. The experimental stress and strain results of the uniaxial tension tests were converted to true stress and logarithmic plastic strain as inputs for the simulation using the following equations:

$$\sigma_{\text{true}} = \sigma_{\text{nom}}(1 + \varepsilon_{\text{nom}}), \tag{6}$$

$$\varepsilon_{\text{true}} = \ln(1 + \varepsilon_{\text{nom}}), \tag{7}$$

where ε_{nom} is the nominal or engineering strain and σ_{nom} is the nominal or engineering stress.
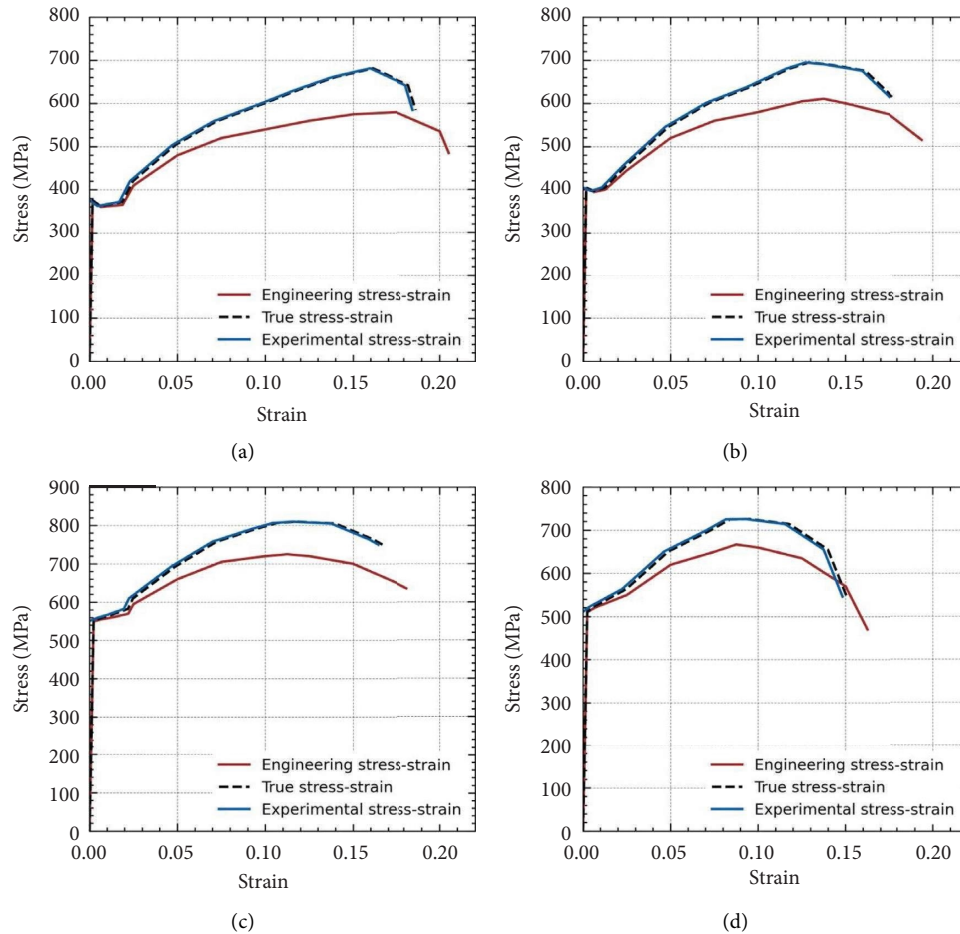
(a)

(b)

(c)

(d)

Figure 2: Stress-strain curves for structural steel and reinforcement: (a) flange section; (b) web section; (c) longitudinal reinforcement; (d) transverse reinforcement.

The steel material properties used for the finite element simulation are given in Table 2.

2.2. Test Specimens' Details. For the current study, an experimentally tested specimen by Lai et al. [1] was utilized as a control for analytical and FEA validation. The behavior of the specimens during the loading was examined based on the failure modes, peak load, and load-deflection plots. A column section given in Figure 3 was utilized as a control in an experimental test conducted by Lai et al. [1]. Analytical and finite element analyses were carried out in this column to investigate the structural performance under compressive load. The variables utilized were the compressive strength of the concrete, the height of the column, and the longitudinal and transverse reinforcement size effects.

3. Numerical Simulation

3.1. General. Basically, the finite element analysis (FEA) requires defining geometry, material properties, assigning a mesh, analysis type, and boundary conditions for a given model. Finite element analysis (FEA) resulted in refined results during the investigation of the flexural, fatigue, and axial performance of composite columns [20, 25, 42, 57]. The studies show that FEA is the best tool to understand the failure mechanism of a structural element under a given loading condition and even helps to predict the performance of structures under complex boundary, load, and geometrical conditions. Both material and geometric nonlinearity were considered in the analysis. The load was applied using several load increments during the simulation. This helps the structure to remain in equilibrium by controlling nonlinear fluctuations in the structure's stiffness at the end of each increment [24].

3.2. Finite Element Modeling of Encased Composite Column. The modeling procedures for each constituent part of an encased composite column were described one by one in this section. The encased composite column is composed of a structural steel section, longitudinal reinforcement, transverse reinforcement, and concrete. The concrete and structural steel are modeled using a three-dimensional 8-noded hexahedral (brick) element with reduced integration (C3D8R). This helps the shear-locking effect during loading

TABLE 2: Steel material data [1].

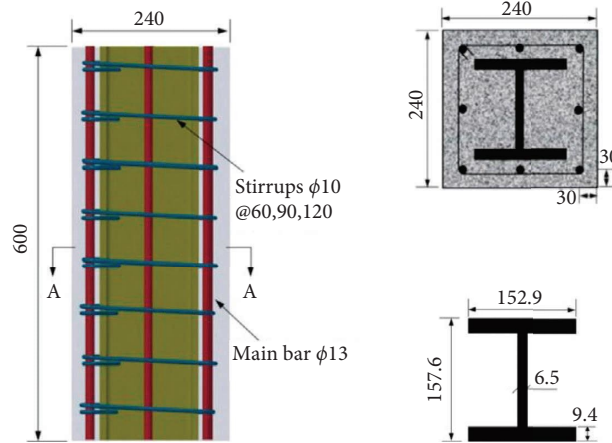| Material		Yield stress (MPa)	Ultimate stress (MPa)	Density (kg/m³)	Young's modulus (MPa)	Poisson's ratio
Steel sections	Flange	375	580	7,850	226,600	0.3
	Web	404	611	7,850	223,900	0.3
Reinforcement bars	Rebar	550	725	7,850	228,200	0.3
	Stirrup	510	667	7,850	197,700	0.3

FIGURE 3: Dimension details of specimen [1].

[34]. For the reinforcement, the T3D2 element was used [53]. The assembled view of the column is depicted in Figure 4.

3.3. Loading and Boundary Conditions.

The FEA model was created based on the experimental setup as shown in Figure 5. The bottom end of the column was fixed, and the axial load was applied through a rigid body reference node at the center of the top loading plate. The rotations and horizontal translations at the top surface were fixed, and translation along the longitudinal downward direction was allowed. The displacement control technique was used to apply the compressive crushing through the reference node at the center of the top loading plate. Figure 5 depicts the experimental setup, boundary, and loading conditions of the current study.

3.4. Interactions Properties.

Kinematic relationships were considered to ensure compatibility between interacting bodies. The first interaction type used was an embedded constraint. The embedded constraint was defined for the interaction between concrete, structural steel, and reinforcement bar. The reinforcement bars and the structural steel were embedded under the concrete. Previous studies also stated that this option ensures a perfect bond between the concrete and embedded parts under the concrete [53, 58]. The concrete was defined as the host region, and the steel sections were defined as the embedded elements. The interaction between the encased composite column and the support and loading plate is defined as a tie. Another interaction type used in this study is general

surface-to-surface contact, which is used to define two contacting bodies in general [24].

3.5. Mesh.

Finite element results are highly dependent on mesh types, control, and sizes. Studies showed that the provision of coarse mesh yielded brittle failures [59–62]. The mesh size is one of the factors contributing to the convergence criteria. It has been also reported that mesh fineness and coarseness have a significant effect on computation time [58, 63–66]. The guideline for maximum mesh size was already stated in the previous report [58, 67]. However, the fines of mesh are usually determined by the convergence of results and practical considerations. A mesh size of 20 mm was used in this study.

4. Result and Discussion

4.1. Manual Verification According to Eurocode 4.

Before conducting the finite element analysis, the result from experimental work was verified by using manual calculation according to Eurocode 4 [30] for the composite column. Thus, the steps to design encased steel columns subjected to axial load are given as follows:

(1) Calculate the ultimate axial load, N_{Ed}

(2) Select a trial section and calculate geometrical properties

(3) Determine the buckling length of the column, L_e

(4) Determine effective flexural stiffness, EI_{eff}
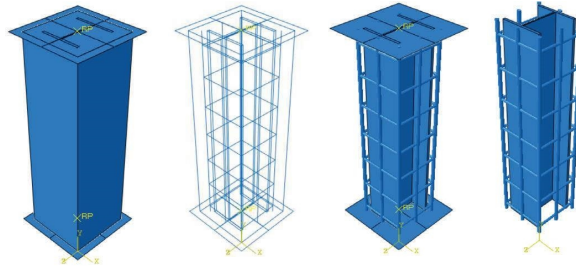
(5) Determine plastic resistance, $N_{pl,Rk}$

FIGURE 4: Assembled FEA model of encased composite column components.

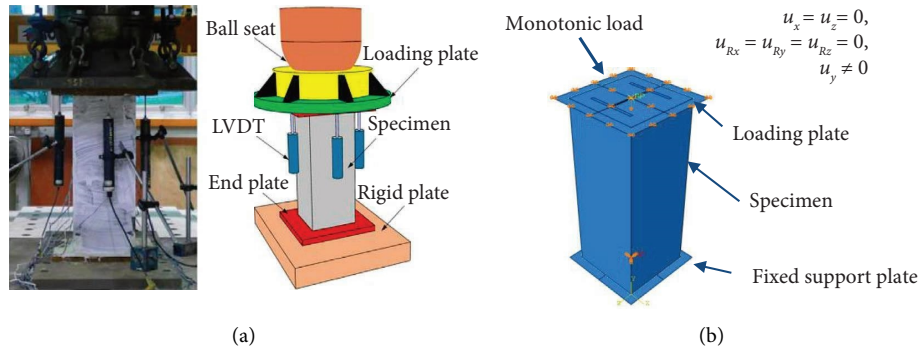(a)   (b)

FIGURE 5: Experimental setup and boundary condition: (a) experimental test setup and instrumentations [1]; (b) FEA boundary conditions.

(6) Determine the relative slenderness of the section (λ)

(7) Choose the buckling curve and compute the reduction factor, χ

(8) Determine buckling resistance, $N_{b,Rd}$

(9) Check if $N_{Ed} < N_{b,Rd}$, else return to step 2

4.1.1. Given Data

N_{Ed} = 4475.4kN

Steel section UC152 × 152 × 30.

Column cross-section, $A_c = 240 \times 240 \, (\text{mm}^2)$

Characteristic cylindrical compressive strength of concrete, f_{ck} = 50MPa

Longitudinal reinforcement, 8∅13

Steel material properties are given in Table 2

Column height, l = 600mm

4.1.2. Design Checks

(a) Geometrical properties of universal column (UC) section

Area of UC section, A_g = 3830mm^2

Radius of Gyration, i_y = 67.60mm and i_x = 38.30mm
Moment of inertia, I_y = 1748cm^4 and I_z = 560cm^4,
Effective length of the column = Le = 0.7 * L = 0.7 * 600 = 420 mm.

(b) Buckling length of the column (considering the bottom end is fixed and the top end is pinned)

$L_e = 0.7 * l = 0.7 * 600\text{mm} = 420\text{mm}$

(c) Effective flexural stiffness, EI_{eff}, of the composite section

$EI_{eff} = E_a I_a + E_s I_s + 0.6 E_{cm} I_c$
where E_a = elastic modulus of structural steel = 226,600MPa (from Table 2); E_s = elastic modulus of reinforcement = 228,200MPa (from Table 2); E_{cm} = modulus of elasticity of concrete = 22 $(f_{cm}/10)^{0.3}$ (GPa) = 22 * $[(50 + 8)/10]^{0.3}$ = 37,278 MPa (Eurocode 2 [51]); I_a = moment of inertia of structural steel; I_c = moment of inertia of uncracked concrete section = $b * h^3/ 12 = 240 * 240^2 /12 = 2,764.8 * 10^5\text{mm}^4$; I_s = moment of inertia of the 8∅13 reinforcement bars = $8 * \pi * D^4/64 = 11,215.88\text{mm}^4$
Thus,

$$EI_{eff,y} = \left(226,600 * 1748 * 10^4 + 228,200 * 11,215.88 + 0.6 * 37,278 * 2,764.8 * 10^5\right) N.mm^2$$

$$= 10.1475 * 10^{12} N.mm^2,$$

$$EI_{eff,z} = \left(226,600 * 560 * 10^4 + 228,200 * 11,215.88 + 0.6 * 37,278 * 2,764.8 * 10^5\right) N.mm^2$$

$$= 7.4555 * 10^{12} N.mm^2.$$

(8)

(d) Composite section plastic resistance

$$N_{Pl,Rk} = A_g f_y + 0.85 A_C f_{ck} + A_s f_{yk}$$

$$= (3830 * 375 + 0.85 * 240 * 240 * 50 + 1061.86 * 550) = 4468.27 kN.$$

(9)

(e) Relative slenderness of the section

The relative slenderness, $\lambda_i = \sqrt{N_{pl,Rk}/N_{cr}}$, where $N_{cr,i} = \pi^2 (EI)_{eff,i}/L_e^2$

$$N_{cr,y} = \left[\frac{\pi^2 * \left(10.1475 * 10^{12}\right)}{420^2}\right] * 10^{-3} = 567,754.03 \, kN,$$

$$N_{cr,z} = \left[\frac{\pi^2 * \left(7.4555 * 10^{12}\right)}{420^2}\right] * 10^{-3} = 417,136.26 kN,$$

(10)

$$\lambda_y = \sqrt{\frac{4,468.27}{567,754.03}} = 0.089,$$

$$\lambda_z = \sqrt{\frac{4,468.27}{417,136.26}} = 0.1035.$$

(f) Buckling curve and the corresponding reduction factor, χ

Check $h/b = 157.6/157.6 = 1.03 < 1.2,$ and $t_f < 100mm$ (EN 1993-1-12005 [56])

Thus, the buckling curve "b" for the y-y axis and the buckling curve "c" for the z-z axis were selected and $\alpha = 0.34$ for curve "b" and $\alpha = 0.49$ for curve "c" (EN 1993-1-12005 [56]).

Reduction factor, $\chi = 1/\phi + \sqrt{\phi^2 - \lambda_i^2}$

$$\phi = 0.5\left[1 + \alpha(\lambda - 0.2) + \lambda^2\right],$$

$$\phi_y = 0.5\left[1 + 0.34(0.089 - 0.2) + 0.089^2\right] = 0.485,$$

$$\phi_z = 0.5\left[1 + 0.49(0.1035 - 0.2) + 0.1035^2\right] = 0.482.$$

(11)

Hence,

$$\chi_y = \frac{1}{0.485 + \sqrt{0.485^2 - 0.089^2}} = 1.04,$$

$$\chi_z = \frac{1}{0.482 + \sqrt{0.482^2 - 0.1035^2}} = 1.05,$$

(12)

χ_y, yields the critical resistance.

(g) Determine the buckling resistance, $N_{b,Rd}$

$N_{b,Rd} = \chi_y * N_{Pl,Rk} = 1.04 * 4468.27 kN = 4647.00 kN$

(h) Check if $N_{Ed} < N_{b,Rd}$

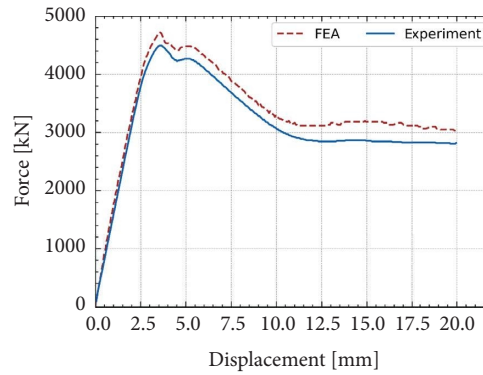$N_{Ed} < N_{b,Rd} \longrightarrow 4475.40 \text{kN} < 4647.00 kN,$

FIGURE 6: Comparative study between FEA and experimental test.

The deviation between the manual calculation and the experimental test becomes

$$\longrightarrow \left(\frac{4647.00 - 4475.40}{4647.00}\right) * 100\% = 3.7\%. \quad (13)$$

For this calculation, it can be seen that the experimental test fairly validates the analytical solution.

4.2. Finite Element Analysis Validation Study. To validate finite element analysis, an experimental work reported by Lai et al. [1] was used as a benchmark experiment. The encased composite column has a cross-section of 240×240 mm dimension with 600 mm height. A total of $8\varnothing 13$ longitudinal reinforcement bars were provided, giving a reinforcement ratio of 1.84%. The transverse bars of $\varnothing 13$ with a clear spacing of 120 mm, giving the volumetric ratio of 1.29% were used. The UC152 × 152 × 30 British steel section was adopted, which accounts for 6.56% of the entire section. This structural steel section is classified as class 1 according to EN1993-1-1, 2005 [56]. The characteristic cylindrical compressive strength of concrete is 50 MPa. The relevant material properties for the finite element analysis are presented in Section 2 under Tables 1 and 2. Furthermore, the finite element analysis instrumentation and modeling parameters are also depicted in Section 3.

In this study, a mesh size of 20 mm fairly validates the experimental work. Results showed that the finite element analysis resulted in a close prediction of the experimental test with an accuracy of 95.20% for the ultimate load-carrying capacity of the encased composite column. The ultimate load obtained from finite element analysis (FEA) and experimental test were 4475.4 kN and 4701.01 kN, respectively. The deviation between the FEA and the experimental test is about 4.80%, which is within an acceptable range. Moreover, the comparative study shown in Figure 6 shows that the simulation fairly traces the postfailure behavior of the encased composite column from the experimental test. Therefore, it has been observed that this validation result becomes a good starting point for the discussed parametric studies in the next sections.

4.3. Effects of Concrete Strength. Obviously, it is a known fact that an increase in compressive strength yields enhanced load-carrying capacity of concrete structures; however, it is difficult to predict how much damage to the concrete matrix is minimized by improving the compressive strength of concrete. Thus, finite element analysis shows very precise information about how much of the concrete matrix is damaged at a given ultimate load. The geometrical and material properties used for the structural steel and reinforcement bar are identical to those given in Section 4.2. Figure 7 clearly shows the effect of concrete strength on the damage characteristics of an encased composite column. The damage to the concrete is significantly minimized due to the increased strength of the concrete. The load-carrying capacity of the encased composite column increased with the increase in concrete compressive strengths, as shown in Figure 8. The load-carrying capacity of the column improved by about 6.38% and 5.93% for the concrete grades of $f_{ck} = 25$ to $f_{ck} = 30$ and $f_{ck} = 30$ to $f_{ck} = 35$, respectively. The capacity of the column improved by 11.93% on average as the compressive strength of concrete increased from $f_{ck} = 25$ to $f_{ck} = 35$, as depicted in Figure 8(b). From this study, we can understand that the damage to the concrete matrix can be minimized by increasing the compressive strength of the concrete. Furthermore, an increase in concrete strength improves the load-bearing capacity of an encased composite column, as expected.

4.4. Effects of Reinforcement Ratio. The effect of longitudinal reinforcement is better understood by observing equivalent plastic strain (PEEQ), as shown in Figures 9(a)–9(c). Keeping other parameters constant, an increase in the reinforcement ratio minimizes the equivalent plastic strain both in structural steel and reinforcement bars. The ultimate load of the encased composite column increased with the increase in reinforcement ratio, as shown in Figure 10. The finite element analysis also verified that the plastic resistance to compression of the composite section is directly proportional to the area of the reinforcing bar, as discussed in Section 4.1. The load-carrying capacity of the column improved by about 4.14% and 4.77%, for an increase in
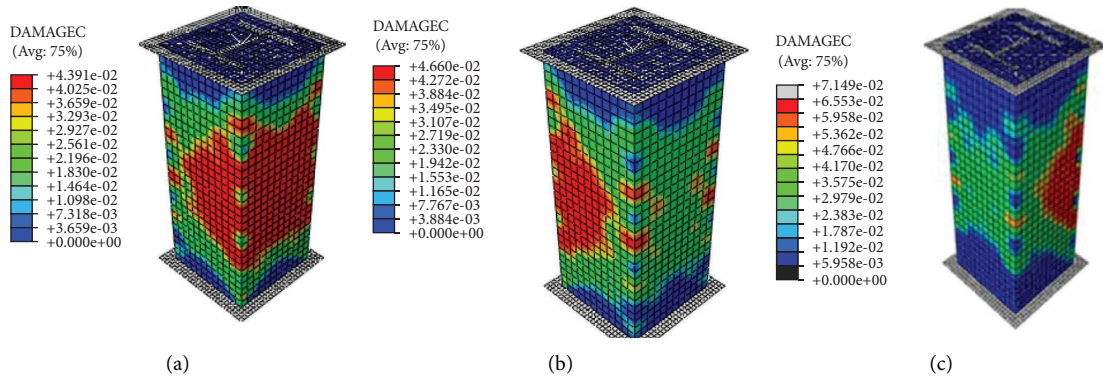
(a)   (b)   (c)

FIGURE 7: Effects of concrete strength on damage characteristics of the encased composite column: (a) f_{ck} = 25; (b) f_{ck} = 30; (c) f_{ck} = 35.
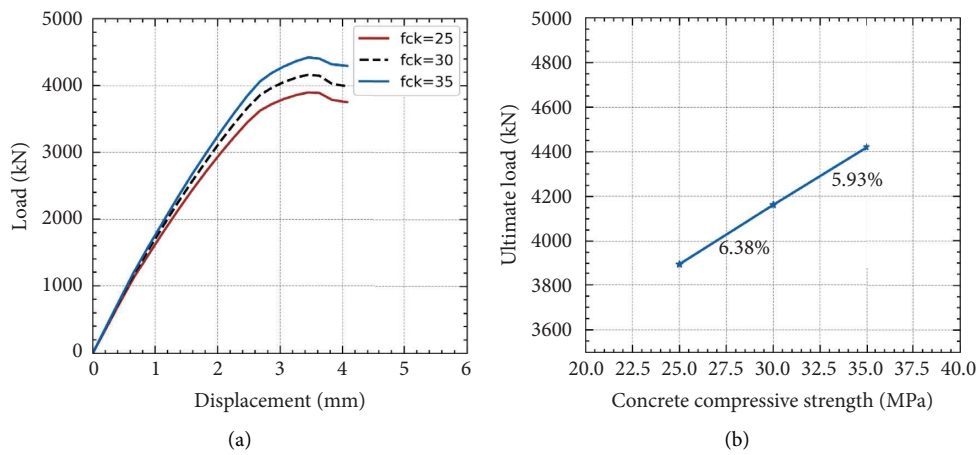

(a)

(b)

FIGURE 8: Comparative study: (a) load versus displacement study; (b) comparison in percentage.

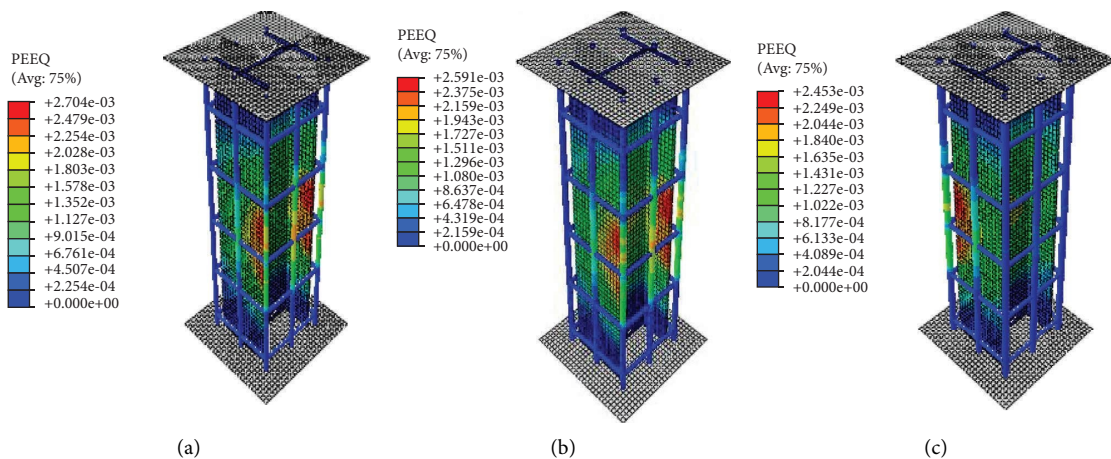(a)   (b)   (c)

FIGURE 9: Effects of reinforcement ratio on damage characteristics of the encased composite column: (a) 0.0157; (b) 0.0214; (c) 0.0279.

reinforcement ratio from 0.0157 to 0.0214 and 0.0214 to 0.0279, respectively. The capacity of the column improved by 8.91% on average when the reinforcement ratio increased from 0.0157 to 0.0279 while keeping the number of bars and other parameters constant, as depicted in Figure 9(b). Thus, from this study, we can understand that an increase in reinforcement ratio minimizes the plastic strain under structural steel and reinforcing bars in fully encased steel
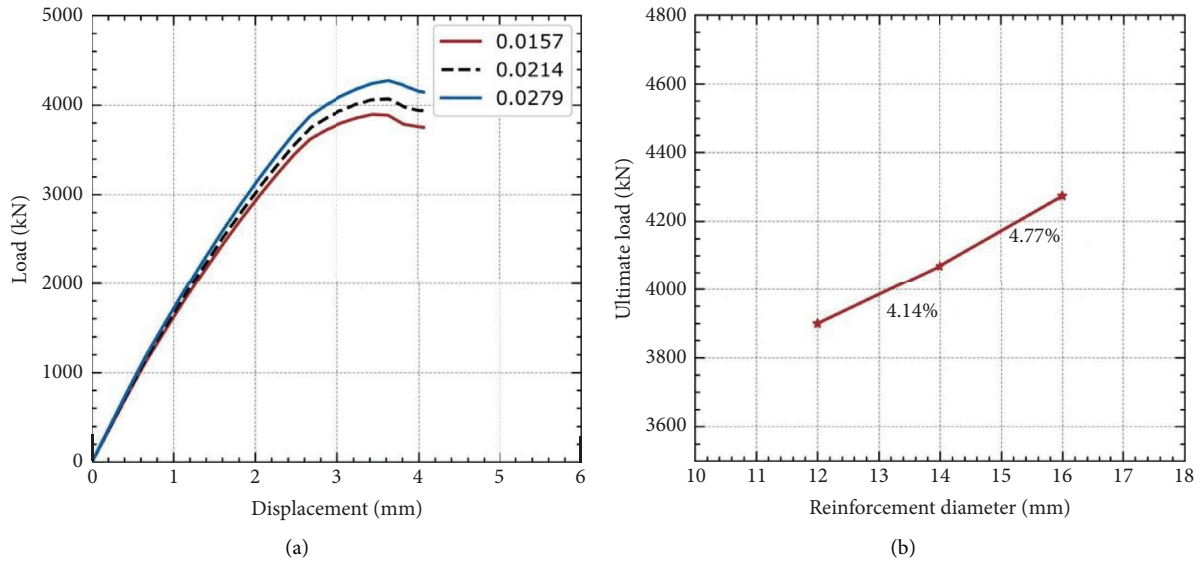
(a)

(b)

FIGURE 10: Comparative study for reinforcement effect(a) load versus displacement study; (b) comparison in percentage.

composite columns. A recent study also depicted that an increase in the reinforcement ratio tends to increase the ultimate load-carrying capacity [68].

5. Conclusions

In this study, nonlinear 3D finite element modeling of square-encased composite columns under monotonic axial compression load was performed. The concrete material was modeled using concrete damage plasticity (CDP), which incorporates the hardening and softening behaviors, and the steel was modeled using metal plasticity. The effects of concrete strength and reinforcement ratio were investigated to understand the capacity and stress-strain distribution under the composite column. The analysis result from the current study fairly validates the experimental result by capturing the postsoftening part of the test specimen. Furthermore, the result from experimental work was verified prior to FEA by using manual calculation according to Eurocode 4 and a simplified method to design encased steel columns under axial compression. Based on the analysis and discussion presented in this study, the following conclusions were drawn:

(i) A comparative study was conducted for finite element analysis to estimate the ultimate load-carrying capacity between analytical calculation according to Eurocode 4 and experiment test. It has been observed that the finite element analysis resulted in a close prediction of the experimental test with an accuracy of 95.20% for the ultimate load-carrying capacity of the encased composite column.

(ii) It has been observed that an appropriate material definition and mesh size selection during finite element analysis (FEA) helps to obtain refined postsoftening failure behavior of the composite volume form load versus displacement plot.

(iii) The increase in the compressive strength of concrete yields a reduction in the damage to the concrete matrix and improves the load-carrying capacity of the composite column. It has been observed that the capacity of the column improved by 11.93% on average as the compressive strength of concrete increased from $f_{ck} = 25$ to $f_{ck} = 35$ by keeping other parameters constant.

(iv) An increase in reinforcement ratio minimizes the equivalent plastic strain both in structural steel and reinforcement bar, and it has been observed that the plastic resistance to compression of the composite section is directly proportional to the area of the reinforcing bar. The capacity of the column improved by 8.91% on average when the diameter of the bar increased from 0.0157 to 0.0279 while keeping the number of bars and other parameters constant.

(v) In general, nonlinear 3D finite element modeling is the finest tool to investigate the performance and damage behavior of composite structures by incorporating correct material modeling.

Data Availability

The data used to support the findings of this study are presented in the manuscript.

Conflicts of Interest

The authors declare that they have no conflicts of interest.

References

[1] B. Lai, J. R. Liew, and M. Xiong, "Experimental study on high strength concrete encased steel composite short columns," *Construction and Building Materials*, vol. 228, Article ID 116640, 2019.

[2] B. Lai and J. R. Liew, "Axial-moment interaction of high strength concrete encased steel composite

columnsexperimental investigation," *Journal of Constructional Steel Research*, vol. 175, Article ID 106370, 2020.

[3] B. Lai, J. R. Liew, and A. L. Hoang, "Behavior of high strength concrete encased steel composite stub columns with C130 concrete and S690 steel," *Engineering Structures*, vol. 200, Article ID 109743, 2019.

[4] B. Lai, J. Richard Liew, and T. Wang, "Buckling behaviour of high strength concrete encased steel composite columns," *Journal of Constructional Steel Research*, vol. 154, pp. 27–42, 2019.

[5] P. Collin, M. Nilsson, and J. Häggström, *International workshop on Eurocode 4-2, Composite Bridges*, Lulea University of Technology, Lulea, Sweden, 2011.

[6] V. M. Karbhari and L. Zhao, "Use of composites for 21st century civil infrastructure," *Computer Methods in Applied Mechanics and Engineering*, vol. 185, no. 2-4, pp. 433–454, 2000.

[7] M. Kazem Sharbatdar, A. Kheyroddin, and E. Emami, "Cyclic performance of retrofitted reinforced concrete beam-column joints using steel prop," *Construction and Building Materials*, vol. 36, pp. 287–294, 2012.

[8] D. K. Kim, *A Database For Composite Columns*, Georgia Institute of Technology, Atlanta, GA, USA, 2005.

[9] Y. S. Song, J. R. Youn, and T. G. Gutowski, "Life cycle energy analysis of fiber-reinforced composites," *Composites Part AApplied Science and Manufacturing*, vol. 40, no. 8, pp. 1257–1265, 2009.

[10] J. Y. Oh, D. H. Lee, J. Lee, K. S. Kim, and S. B. Kim, "Experimental study on reinforced concrete column incased in prefabricated permanent thin-walled steel form," *Advances in Materials Science and Engineering*, vol. 2016, Article ID 3806549, 11 pages, 2016.

[11] P. Hopkinson, H. M. Chen, K. Zhou, Y. Wang, and D. Lam, "Recovery and reuse of structural products from end-of-life buildings," *Proceedings of the Institution of Civil Engineers - Engineering Sustainability*, vol. 172, no. 3, pp. 119–128, 2019.

[12] S. Rahman, M. Begum, and R. Ahsan, "Comparison between experimental and numerical studies of fully encased composite columns," *International Journal of Structural and Construction Engineering*, vol. 10, pp. 762–769, 2016.

[13] M. S. Rahman, *Behaviour and Strength of Fully Encased Composite Columns*, pp. 1–198, Bangladesh University Of Engineering And Technology, Dhaka, Bangladesh, 2016.

[14] S. A. Mirza and E. A. Lacroix, "Comparative strength analyses of concrete-encased steel composite columns," *Journal of Structural Engineering*, vol. 130, pp. 1941–1953, 2004.

[15] S. Priya, R. Karthick, and V. Chandrikka, "Review on steel concrete composite column," *International Research Journal of Engineering and Technology*, vol. 6, pp. 450–454, 2019.

[16] J. F. Hajjar, "Composite steel and concrete structural systems for seismic engineering," *Journal of Constructional Steel Research*, vol. 58, no. 5-8, pp. 703–723, 2002.

[17] S. Rahman, M. Begum, and R. Ahsan, "Comparison between experimental and numerical studies of fully encased composite columns," *International Journal of Structural and Construction Engineering*, vol. 10, pp. 756–763, 2016.

[18] Y. F. An, L. H. Han, and C. Roeder, "Flexural performance of concrete-encased concrete-filled steel tubes," *Magazine of Concrete Research*, vol. 66, no. 5, pp. 249–267, 2014.

[19] E. Ellobody and B. Young, "Investigation of concrete encased steel composite columns at elevated temperatures," *Thin-Walled Structures*, vol. 48, no. 8, pp. 597–608, 2010.

[20] E. Ellobody, B. Young, and D. Lam, "Eccentrically loaded concrete encased steel composite columns," *Thin-Walled Structures*, vol. 49, no. 1, pp. 53–65, 2011.

[21] C. Dundar, S. Tokgoz, A. K. Tanrikulu, and T. Baran, "Behaviour of reinforced and concrete-encased composite columns subjected to biaxial bending and axial load," *Building and Environment*, vol. 43, no. 6, pp. 1109–1120, 2008.

[22] C. S. Kim, H. G. Park, K. S. Chung, and I. R. Choi, "Eccentric axial load testing for concrete-encased steel columns using 800 MPa steel and 100 MPa concrete," *Journal of Structural Engineering*, vol. 138, no. 8, pp. 1019–1031, 2012.

[23] T. H. Shih, C. C. Chen, C. C. Weng, S. Y. L. Yin, and J. C. Wang, "Axial strength and ductility of square composite columns with two interlocking spirals," *Journal of Constructional Steel Research*, vol. 90, pp. 184–192, 2013.

[24] K. Z. Mulgeta Mersha and E. C. Agon, *Investigation on Effect of Different Steel Section on the Performance of Encased Composite Column*, Jimma Institute of Technology, Jimma University, Jimma, Ethiopia, 2020.

[25] L. H. Han, F. Y. Liao, Z. Tao, and Z. Hong, "Performance of concrete filled steel tube reinforced concrete columns subjected to cyclic bending," *Journal of Constructional Steel Research*, vol. 65, no. 8-9, pp. 1607–1616, 2009.

[26] W. W. Qian, W. Li, L. H. Han, and X. L. Zhao, "Analytical behavior of concrete-encased CFST columns under cyclic lateral loading," *Journal of Constructional Steel Research*, vol. 120, pp. 206–220, 2016.

[27] W. L. A. de Oliveira, S. De Nardin, A. L. H. de Cresce El Debs et al., "Influence of concrete strength and length/diameter on the axial capacity of CFT columns," *Journal of Constructional Steel Research*, vol. 65, no. 12, pp. 2103–2110, 2009.

[28] S. A. Mirza, "Parametric study of composite column strength variability," *Journal of Constructional Steel Research*, vol. 14, no. 2, pp. 121–137, 1989.

[29] Y. Li, X. Wu, X. Lis, K. Zhang, and C. Gao, "Compression performance and calculation method of thin-walled prefabricated steel tube lightweight concrete columns," *Advances in Civil Engineering*, vol. 2022, p. 11, 2022.

[30] Eurocode 4:, "Standard Design of Composite Steel and Concrete Structures - Part 1-1 General Rules and Rules for Buildings," *European Committee for Standardization*, Brussels, Belgium, 2004.

[31] D. H. Nguyen and W. K. Hong, "Part I failure criteria of the steel-concrete columns (SRC columns) confined by cross-shaped flange sections," *Journal of Asian Architecture and Building Engineering*, vol. 20, no. 2, pp. 179–192, 2021.

[32] M. H. Lai and J. C. M. Ho, "Confinement effect of ring-confined concrete-filled-steel-tube columns under uni-axial load," *Engineering Structures*, vol. 67, pp. 123–141, 2014.

[33] M. Begum, R. G. Driver, and A. E. Elwi, *Numerical Simulations of the Behaviour of Partially Encased Composite Columns*, Heritage, Canada, 2007.

[34] M. K. I. Khan, C. K. Lee, and Y. X. Zhang, "Parametric study on high strength ECC-CES composite columns under axial compression," *Journal of Building Engineering*, vol. 44, Article ID 102883, 2021.

[35] B. Lai, J. R. Liew, A. Venkateshwaran, S. Li, and M. Xiong, "Assessment of high-strength concrete encased steel composite columns subject to axial compression," *Journal of Constructional Steel Research*, vol. 164, Article ID 105765, 2020.

[36] C. Kim, H. Park, M. Asce, K. Chung, and I. R. Choi, "Eccentric axial load capacity of high-strength steel-concrete composite columns of various sectional shapes," *Journal of Structural Engineering*, vol. 140, no. 4, 2014.

[37] D. Y. Wu, L. Z. Sun, F. Yang, J. L. Zhao, and W. Li, "Axial compressive behavior of square reinforced concrete columns

confined using two layers of stirrups," *Advances in Structural Engineering*, vol. 19, no. 8, pp. 1345–1356, 2016.

[38] R. Hindi, M. Al-Qattawi, and A. Elsharief, "Influence of Different Confinement Patterns on the Axial Behavior of R/C Columns," in *Proceedings of the Structures Congress 2005*, New York, NY, USA, April 2005.

[39] C. Y. Liang, C. C. Chen, C. C. Weng, S. Y. L. Yin, and J. C. Wang, "Axial compressive behavior of square composite columns confined by multiple spirals," *Journal of Constructional Steel Research*, vol. 103, pp. 230–240, 2014.

[40] L. Jin, L. Fan, P. Li, and X. Du, "Size effect of axial-loaded concrete-filled steel tubular columns with different confinement coefficients," *Engineering Structures*, vol. 198, 2019.

[41] J. Zhang, X. Li, W. Cao, and C. Yu, "Cyclic behavior of steel tube-reinforced high-strength concrete composite columns with high-strength steel bars," *Engineering Structures*, vol. 189, pp. 565–579, 2019.

[42] Y. R. Abbas, "Nonlinear finite element analysis to the circular CFST stub columns," *Procedia Engineering*, vol. 173, pp. 1692–1699, 2017.

[43] E. Ellobody and B. Young, "Numerical simulation of concrete encased steel composite columns," *Journal of Constructional Steel Research*, vol. 67, no. 2, pp. 211–222, 2011.

[44] M. Begum, R. G. Driver, and A. E. Elwi, "Behaviour of partially encased composite columns with high strength concrete," *Engineering Structures*, vol. 56, pp. 1718–1727, 2013.

[45] M. K. I. Khan, C. K. Lee, and Y. X. Zhang, "Numerical modelling of engineered cementitious composites-concrete encased steel composite columns," *Journal of Constructional Steel Research*, vol. 170, Article ID 106082, 2020.

[46] G. Tunc, M. M. Othman, and H. C. Mertol, "Finite element analysis of frames with reinforced concrete encased steel composite columns," *Buildings*, vol. 12, no. 3, p. 375, 2022.

[47] T. A. Mohammed and S. Abebe, "Numerical investigation on cfrp strengthening and reinforcement bar detailing of rc columns to resist blast load," *SSRN Electronic Journal*, vol. 8, 2022.

[48] B. Ahmed, K. Zerfu, and E. C. Agon, "Construction of uniaxial interaction diagram for slender reinforced concrete column based on nonlinear finite element analysis," *Advances in Civil Engineering*, vol. 2021, Article ID 3275512, 10 pages, 2021.

[49] B. Lai, J. Y. R. Liew, and S. Li, "Finite element analysis of concrete-encased steel composite columns with off-center steel section," in *Proceedings of the 12th International Conference on Advances in Steel-Concrete Composite Structures*, pp. 297–303, Valencia, Spain, June 2018.

[50] K. D. Tsavdaridis, C. D'Mello, and B. Y. Huo, "Experimental and computational study of the vertical shear behaviour of partially encased perforated steel beams," *Engineering Structures*, vol. 56, pp. 805–822, 2013.

[51] BSI, *Eurocode 2Design of concrete Structures -Part 1-1 General Rules and Rules for Buildings*British Standards Institution, London, UK, 2004.

[52] M. A. Najafgholipour, S. M. Dehghan, A. Dooshabi, and A. Niroomandi, "Finite element analysis of reinforced concrete beam-column connections with governing joint shear failure mode," *Latin American Journal of Solids and Structures*, vol. 14, pp. 1200–1225, 2017.

[53] Abaqus/CAE User's Manual 6.14, "Dassault Systemes," *Simulia Corpia Corp*, Providence, USA, 2014.

[54] W. Wahalathantri, D. Thambiratnam, T. Chan, and S. Fawzia, "A material model for flexural crack simulation in reinforced concrete elements using ABAQUS," in *Proceedings of the first international conference on engineering, designing and developing the built environment for sustainable wellbeing*, pp. 260–264, Australia, January 2011.

[55] M. Hafezolghorani, F. Hejazi, S. Lecturer, R. Vaghei, M. Saleh, and B. Jaafar, "Simplified Damage Plasticity Model for Concrete," *Structural Engineering International*, vol. 27, 2017.

[56] Eurocode 3, "Design of steel structures - Part 1-1: General rules and rules for buildings," *European Committee for Standardization*, Brussels, Belgium, 2005.

[57] Z. Tao, B. Uy, F. Y. Liao, and L. H. Han, "Nonlinear analysis of concrete-filled square stainless steel stub columns under axial compression," *Journal of Constructional Steel Research*, vol. 67, no. 11, pp. 1719–1732, 2011.

[58] K. Zerfu and J. J. Ekaputri, "Nonlinear finite element study on element size effects in alkali-activated fly ash based reinforced geopolymer concrete beam," *Case Studies in Construction Materials*, vol. 15, 2021.

[59] J. H. Chen, W. F. Xu, R. Z. Xie et al., "Sample size effect on the dynamic torsional behaviour of the 2A12 aluminium alloy," *Theoretical and Applied Mechanics Letters*, vol. 7, no. 6, pp. 317–324, 2017.

[60] Q. Sun, H. Zhu, G. Wang, and J. Fan, "Effects of mesh resolution on hypersonic heating prediction," *Theoretical and Applied Mechanics Letters*, vol. 1, no. 2, Article ID 022001, 2011.

[61] G. B. Barbat, M. Cervera, M. Chiumenti, and E. Espinoza, "Structural size effectexperimental, theoretical and accurate computational assessment," *Engineering Structures*, vol. 213, Article ID 110555, 2020.

[62] K. Zerfu and J. J. Ekaputri, "An approximate deflection function for simply supported quadrilateral thin plate by variational approach," in *Proceedings of the AIP Conference Proceedings*, New York, NY, USA, August2017.

[63] R. Jain, S. K. Pal, and S. B. Singh, *Numerical Modeling Methodologies for Friction Stir Welding Process*, Elsevier, Amsterdam, Netherlands, 2017.

[64] S. Mukhopadhyay and S. R. Hallett, "An augmented cohesive element for coarse meshes in delamination analysis of composites," *Composite Structures*, vol. 254, Article ID 112890, 2020.

[65] K. Wu, Q. Deng, N. Deng, X. Cai, and W. Huang, "Size effects of finite element model for three-dimensional microstructural modeling of asphalt mixture," *Advances in Materials Science and Engineering*, vol. 2019, Article ID 1754567, 9 pages, 2019.

[66] F. Marin, A. F. d. Souza, R. G. Pabst, and C. H. Ahrens, "Influences of the mesh in the CAE simulation for plastic injection molding," *Polimeros*, vol. 29, no. 3, 2019.

[67] B. B. M. A. N. Hendriks and A. de Boer, "Guidelines for nonlinear finite element analysis of concrete structures F020," in *Rijkswaterstaat Tech. Doc*, pp. 1–69, 2017.

[68] K. Zerfu and J. J. Ekaputri, "The effect of reinforcement ratio on the fl exural performance of alkali-activated fl y ash-based geopolymer concrete beam," *Heliyon*, vol. 8, no. 12, 2022.